Zhao *et al. Ageing Neur Dis* 2024;4:8
DOI: 10.20517/and.2023.31

Ageing and Neurodegenerative Diseases

Original Article

Open Access

Check for updates

Automatically targeting the dorsolateral subthalamic nucleus for functional connectivity-guided rTMS therapy

Na Zhao[1,2,3,4,5,#], Yang Qiao[1,2,3,5,6,#], Juan Yue[1,2,3,#], Ying Jing[1,2,3], Qiu Ge[1,2,3], Meng Zhang[1,2,3], Jianguo Zhang[7], Yuan Zhen[5,6], Yu-Tao Xiang[4,5,*], Jue Wang[8,*], Yu-Feng Zang[1,2,3,*]

[1]Center for Cognition and Brain Disorders, the Affiliated Hospital of Hangzhou Normal University, Hangzhou 310015, Zhejiang, China.
[2]Institute of Psychological Sciences, Hangzhou Normal University, Hangzhou 311121, Zhejiang, China.
[3]Zhejiang Key Laboratory for Research in Assessment of Cognitive Impairments, Hangzhou 310015, Zhejiang, China.
[4]Unit of Psychiatry, Department of Public Health and Medicinal Administration, & Institute of Translational Medicine, Faculty of Health Sciences, University of Macau, Macao 999078, China.
[5]Centre for Cognitive and Brain Sciences, University of Macau, Macao 999078, China.
[6]Faculty of Health Sciences, University of Macau, Macao 999078, China.
[7]Department of Neurosurgery, Beijing Tiantan Hospital, Capital Medical University, Beijing 100070, China.
[8]Institute of sports medicine and health, Chengdu Sport University, Chengdu 610041, Sichuan, China.
[#]Authors contributed equally.

[*]**Correspondence to:** Prof. Yu-Feng Zang, Institute of Psychological Sciences, Hangzhou Normal University, No. 2318, Yuhangtang Rd, Cangqian, Yuhang District, Hangzhou 311121, Zhejiang, China. E-mail: zangyf@hznu.edu.cn; Dr. Jue Wang, Institute of sports medicine and health, Chengdu Sport University, No. 2, Tiyuyuan Rd, Wuhou District, Chengdu 610041, Sichuan, China. E-mail: juefirst@cdsu.edu.cn; Prof. Yu-Tao Xiang, Unit of Psychiatry, Department of Public Health and Medicinal Administration, & Institute of Translational Medicine, Faculty of Health Sciences, University of Macau, Avenida da Universidade, Taipa, Macau 999078, China. E-mail: ytxiang@um.edu.mo

How to cite this article: Zhao N, Qiao Y, Yue J, Jing Y, Ge Q, Zhang M, Zhang J, Zhen Y, Xiang YT, Wang J, Zang YF. Automatically targeting the dorsolateral subthalamic nucleus for functional connectivity-guided rTMS therapy. *Ageing Neur Dis* 2024;4:8. https://dx.doi.org/10.20517/and.2023.31

Received: 21 Jul 2023 **First Decision:** 16 Apr 2024 **Revised:** 24 Apr 2024 **Accepted:** 6 May 2024 **Published:** 13 May 2024

Academic Editors: Weidong Le, David Finkelstein **Copy Editor:** Pei-Yun Wang **Production Editor:** Pei-Yun Wang

Abstract

Aim: Many resting-state functional magnetic resonance imaging (rs-fMRI) studies have provided evidence that repetitive transcranial magnetic stimulation (rTMS) exerts treatment effects via functional connectivity (FC) from a superficial stimulation target to a deep effective region. The dorsolateral subthalamic nucleus (DL-STN) is an effective target in deep brain stimulation surgery for Parkinson's disease (PD), but its targeting highly depends on

well-trained neurosurgeons and is not easily used for FC-guided rTMS. We aimed to devise a method for automatically localizing the DL-STN, and further develop a one-stop plug-in of rs-fMRI FC analysis to assist future individualized FC-guided rTMS.

Methods: Based on structural and iron-sensitive MRI of 78 participants, two raters defined the DL-STN coordinates with very high reliability. The averaged coordinates in the standard Montreal Neurological Institute (MNI) space were: left DL-STN, x: -11.89 ± 0.82, y: -14.51 ± 1.00, and z: -6.40 ± 1.01 and the right DL-STN, x: 12.53 ± 0.77, y: -13.97 ± 0.86, and z: -6.57 ± 0.99. As the individual distances from the averaged coordinates were less than 3 mm (within one voxel for most rs-fMRI studies) for all 78 participants, we defined the average coordinates as AutoSTN. We then developed a one-stop plug-in named Connectivity and Coordinates Converting Assistant Toolbox (CC-CAT) and performed AutoSTN FC analysis.

Results: The AutoSTN seed showed significant FC with the motor cortices in all participants.

Conclusion: The AutoSTN-based rs-fMRI FC could guide future rTMS on PD. The one-stop plug-in CC-CAT can be used for any FC-guided rTMS treatment.

Keywords: Dorsolateral subthalamic nucleus, automatic targeting, Parkinson's disease, functional connectivity, repetitive transcranial magnetic stimulation

INTRODUCTION

Parkinson's disease (PD), one of the most frequent neurodegenerative disorders, is clinically characterized by akinesia, rigidity, resting tremor, and gait instability and is accompanied by various nonmotor complications, such as depression, cognitive decline, and sleeping problems, all of which could lead to significant family and social burdens[1,2]. Although dopaminergic drugs could effectively control motor symptoms at the early stage of PD, nonmotor symptoms might be worsened, and additional drug-related motor complications could emerge with long-term dopaminergic treatment[3,4]. Deep brain stimulation (DBS) surgery is a well-established and effective antiparkinsonian method for those patients who are refractory to medications, but it has a high cost and depends on strict patient selection criteria[5].

As a noninvasive technique, repetitive transcranial magnetic stimulation (rTMS) has been recommended for the treatment of PD[5-7]. While the commonly used figure "8" coil offers a focused stimulation approach, its focus could only reach 2~4 cm in depth[8-10], i.e., only the superficial cortex could be stimulated directly. However, the core pathology of most brain disorders, including PD[11], lies in the deep brain regions. Effectively modulating deep brain activity through the superficial cortex is essential for rTMS treatment. Wang *et al.* proposed a functional connectivity (FC)-guided rTMS approach with stimulation of the left parietal cortex which has FC with the hippocampus. The authors successfully modulated the FC of the hippocampus and significantly improved subjects' associative memory performance[12]. This FC-guided rTMS approach might also be a promising therapy for patients with brain disorders.

The sensorimotor subdivision of the subthalamic nucleus (STN), a crucial node of the cortico-basal ganglia motor pathway[13,14], is an effective deep brain target in DBS surgery for PD patients[15-17]; the effectiveness of targeting this region indicates that the dorsolateral (DL)-STN might be a viable deep brain region in the FC-guided rTMS approach.

However, the small size, biconvex shape, oblique orientation in 3D planes, and special junctional position among deep brain regions of the DL-STN[18-20] make it a challenge to precisely target this region. To address

the issue in DBS surgery, a method based on the anatomical landmarks of the red nucleus (RN) is widely used[21,22]. This method greatly depends on well-trained neurosurgeons and is not suitable for FC-guided rTMS.

Therefore, the current study developed an "AutoSTN" method to help automatically target DL-STN coordinates. Furthermore, a one-stop plug-in FC analytic toolbox named the "Connectivity and Coordinates Converting Assistant Toolbox (CC-CAT)" was developed to automatically target the DL-STN in native space and to serve as an individualized potential superficial stimulation target in rTMS therapy.

METHODS

Participants and data acquisition

The research was conducted at the Center for Cognition and Brain Disorders (CCBD) of Hangzhou Normal University (HZNU) and subjected to a rigorous review by the local ethics committee (No. 20140508). Recruited participants excluded those with a history of neurological and psychiatric disorders. For each subject, a written informed consent was signed before participation in this study. Eighty subjects were included in this study. Of these, two were excluded due to poor MRI image quality; thus, 78 subjects (60.9 ± 7.7 years old, 54 males) were finally included.

For all participants, a resting-state functional magnetic resonance imaging (rs-fMRI), 3D-enhanced susceptibility-weighted angiography (ESWAN), and 3D T1-weighted imaging scanning were collected on a 3T GE scanner (MR750, GE Medical Systems, Milwaukee, WI).

During rs-fMRI collection, the subjects were instructed to keep their eyes closed, avoid falling asleep, and remain as still as possible. The rs-fMRI images were scanned with the following parameters: repetition time (TR) = 2,000 ms, echo time (TE) = 30 ms, interleaved acquisition with a total of 43 slices, flip angle (FA) = 90°, collecting matrix = 64 × 64, field of view (FOV) = 220 × 220 mm^2, spatial resolution = 3.44 × 3.44 × 3.20 mm^3, and total scanning time = 8 min. ESWAN was performed as follows: TR = 54 ms, 16 echoes, first echo time (TE1) = 3 ms, echo separation = 3 ms, FA = 12°, collecting matrix = 256 × 256, FOV = 256 × 256 mm^2, and spatial resolution = 1 × 1 × 1 mm^3. For the 3D T1 anatomical image, it was collected as follows: TR = 8.1 ms, TE = 3.1 ms, a total of 176 sagittal slices with thickness = 1 mm, FA = 8°, and FOV = 250 × 250 mm^2.

Data preprocessing

Individual DL-STN coordinate targeting based on anatomical landmarks

Data preprocessing for DL-STN coordinate targeting for each subject was performed based on AFNI (https://afni.nimh.nih.gov/) and SPM12 (http://www.fil.ion.ucl.ac.uk/spm/). First, we reoriented the T1 image manually to anterior commissure-posterior commissure (AC-PC) stereotactic space using 3drefit in AFNI. Then, ESWAN image was coregistered to the T1 image using SPM. After that, DL-STN coordinate targeting was conducted two times (1st and 2nd) by two independent raters (ZN and YJ) on the coregistered ESWAN images as follows.

DL-STN coordinate targeting was conducted on the coregistered ESWAN image in AC-PC aligned stereotactic space according to the steps of defining DL-STN in DBS surgery[21,22] using AFNI. The details are shown in Figure 1.

We estimated the intra- (i.e., test-retest) and inter-rater reliability of all the x, y, and z coordinates using the intra-class correlation (ICC) according to the following equation[23,24]:

$$ICC = \frac{MSr - MSe}{MSr + (K-1)MSe + K(MSc - MSe)/n} \quad (1)$$

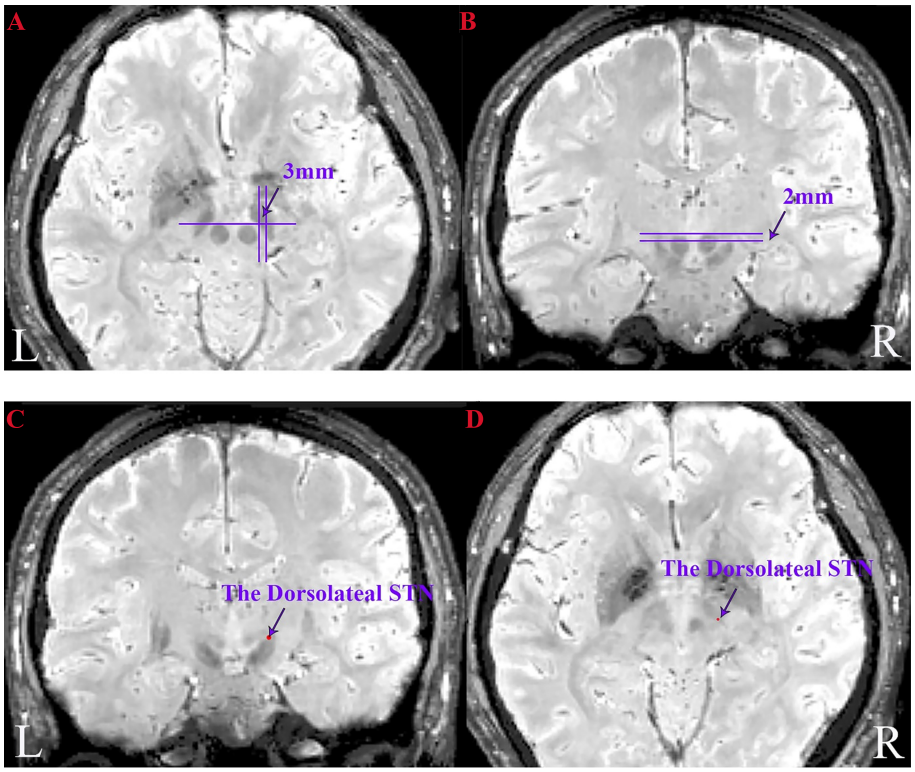

Figure 1. Targeting the DL-STN coordinates of a subject. (A) The axial slice of the red nucleus with the maximal diameter was determined. The *x* coordinate of the DL-STN was defined 3 mm lateral to the lateral edge of the RN. The *y* coordinate was defined as the coordinate of a line tangent to the anterior edge of the RN; (B) The *z* coordinate of the DL-STN was defined 2 mm inferior to the superior edge of the RN. (C) and (D) are the coronal and axial views of the DL-STN coordinates, respectively. DL-STN: Dorsolateral subthalamic nucleus; RN: red nucleus.

where *MSr* represents between-subject variance, *MSe* represents the random error, *MSc* represents between-rater variance, *n* is the number of subjects, and *K* is the number of raters.

Additionally, the intra- and inter-rater Euclidean distances of the *x*, *y*, and *z* coordinates for each subject were calculated.

The coordinates of our results were compared with those of Lozano's DL-STN[22]. It should be noted that the origin of the coordinates in their study was the midpoint of the AC-PC line, and we transformed their coordinate origin to the AC.

The AutoSTN method to define the DL-STN coordinates

All the images, including the labeled image with DL-STN coordinates, were transformed to Montreal Neurological Institute (MNI) space. To estimate the variation in the individual DL-STN coordinates (*x*, *y*, *z*), the distance between the individual and the average MNI coordinates was calculated (i.e., *x*, *y* and *z* coordinates were evaluated separately).

FC of the DL-STN at the group level and individual level

The *x*, *y*, and *z* coordinates displayed high intra- and inter-reliability with very small Euclidean distances [Table 1, Supplementary Figure 1]. Moreover, the distances between the individual and the averaged coordinates were less than 2 mm (*x*, *y* and *z* coordinates) for most subjects (the details are displayed in the

Table 1. The intra- and inter-rater reliability of the DL-STN coordinates

		Left DL-STN			Right DL-STN		
Intra-rater	**Rater**	***x***	***y***	***z***	***x***	***y***	***z***
	R1	0.965	0.991	0.999	0.990	0.993	0.996
	R2	0.981	0.985	0.999	0.987	0.989	0.999
		Left DL-STN			**Right DL-STN**		
Inter-rater	**Time**	***x***	***y***	***z***	***x***	***y***	***z***
	1st	0.950	0.978	0.999	0.953	0.983	0.999
	2nd	0.950	0.971	0.999	0.967	0.975	0.999

DL-STN: Dorsolateral subthalamic nucleus; R1: rater 1 (ZN); R2: rater 2 (YJ); 1st: the first time the DL-STN was targeted; 2nd: the second time the DL-STN was targeted.

"RESULTS" section). Therefore, we defined the average coordinates as the AutoSTN coordinates (DL-STN on the left, x = -11.89 ± 0.82; y = -14.51 ± 1.00; z = -6.40 ± 1.01; DL-STN on the right, x = 12.53 ± 0.77; y = -13.97 ± 0.86; z = -6.57 ± 0.99). The AutoSTN MNI coordinates could not only be used to automatically target the DL-STN coordinates in MNI space but could also be used to achieve automatic DL-STN coordinate targeting in individual native AC-PC stereotactic spaces by transforming the AutoSTN coordinates to those in individual native spaces. This method of automatically targeting the DL-STN is named the "AutoSTN" method.

To validate our assumption that the DL-STN has significant FC with the motor cortices, we conducted group DL-STN FC analysis in MNI space and individual DL-STN FC analysis in native space. All functional data analyses were processed using the DPABI 4.3 toolbox (DPABI_V2.3, http://rfmri.org/dpabi) and validated by using the newly developed plug-in "CC-CAT" (please see "Automatic implementation using the 'CC-CAT' plug-in" section).

For the FC in MNI space, we first preprocessed the images through the following steps: (1) removal of the first 10 time frames; (2) slice-timing correction to correct the slice-dependent delays; and (3) head motion correction. According to the realignment parameter of head movement, the subjects who presented more than 2 mm displacement or 2-degree translation in any of the x, y, or z direction were excluded. Then, we performed: (4) co-registration of fMRI images to the AC-PC aligned T1 images as mentioned in "Individual DL-STN coordinate targeting based on anatomical landmarks" section; (5) normalized images to MNI space using EPI normalization; (6) bandpass filtering of 0.01-0.08 Hz; (7) removal of linear trends and nuisance covariates with head motion (Friston-24), white matter (WM), and cerebrospinal fluid (CSF) parameters; and (8) spatial smoothing using a Gaussian kernel with full-width half maximum (FWHM) = 6 mm. After preprocessing, the time frame of the voxel of the DL-STN (DL-STN on the left, x: -11.89 ± 0.82, y: -14.51 ± 1.00, and z: -6.40 ± 1.01 and DL-STN on the right, x: 12.53 ± 0.77, y: -13.97 ± 0.86, and z: -6.57 ± 0.99) was extracted, and then whole-brain FC analyses were performed for each subject. Additionally, one sample t-tests were performed [Gibbs random field (GRF) correction, individual P < 1E-09, cluster P < 1E-07]. To guide potential FC-guided rTMS treatment, we generated a motor cortex mask (left and right separately) by combining the group-level FC map and the motor cortices [Brodmann area 4 (BA4) and Brodmann area 6 (BA6)] in the Brodmann template.

Considering that FC-guided rTMS would be performed in the native space, we transformed the individual FC maps within the motor cortex mask from MNI space to native space.

Automatic implementation using the "CC-CAT" plug-in

We have developed a one-stop solution, a plug-in named "CC-CAT" based on RESTplus (http://restfmri.net/forum/), for automatic implementation.

In this plug-in, users only need to perform one single click and input a few parameters, i.e., the TR and slice numbers, and the program will automatically perform all the steps we mentioned above.

As Supplementary Figure 2 shows, users need to select the region of interest (ROI) (the DL-STN for this paper), type in the TR and the number of slices in the fMRI data that are included, set the input/output directory, and then just perform a single click on the button labeled "Press to Convert".

The program will write the following results to the output directory [Supplementary Figure 3]:

1. Left and right STN coordinates in native space (text file, i.e., rev_LROI_Coordinate.txt, rev_RROI_Coordinate.txt).
2. Left and right DL-STN masks in native space (NIFTI files with prefixes "rev_LSTN_MNI" and "rev_RSTN_MNI").
3. Left and right STN-based FC map in native space (NIFTI files with prefixes "rev_LROI1FC_" and "rev_RROI2FC_").
4. Left and right STN-based FC map in MNI space (NIFTI files with prefixes "ROI1FC_" and "ROI2FC_").

All the FC analyses mentioned above were validated by using the newly developed plug-in toolbox.

RESULTS

The DL-STN coordinates in the native AC-PC aligned space

The DL-STN coordinates in the native AC-PC aligned space displayed high intra- and inter-rater reliability (ICCs > 0.95, Table 1). The overall intra- and inter-rater Euclidean distances of the *x*, *y*, and *z* coordinates were very small [Supplementary Figure 1]. Three subjects displayed intra-rater distances of 3-4 mm in any direction (*x*, *y*, and *z*) [Table 2], and 8 subjects presented inter-rater distances of 3-4 mm in any direction (*x*, *y*, and *z*) [Table 3].

In native AC-PC aligned space, the DL-STN coordinates (*x*, *y*, and *z*) of our study were consistent with those of Lozano *et al.*, with only the z coordinate being approximately 1 mm inferior to that of Lozano's DL-STN [Supplementary Table 1][22].

The DL-STN coordinates in standard MNI space

Overall, the average coordinates of the DL-STN in standard MNI space were as follows: the left DL-STN, *x*: -11.89 ± 0.82, *y*: -14.51 ± 1.00, and *z*: -6.40 ± 1.01 and the right DL-STN, *x*: 12.53 ± 0.77, *y*: -13.97 ± 0.86, and *z*: -6.57 ± 0.99 [Table 4].

The distances for *x*, *y*, and *z* between the individual DL-STN coordinates and the average DL-STN coordinates were less than 2 mm for 93.6% of subjects [Figure 2]. Five (6.4%) subjects displayed 2-3 mm from the average DL-STN coordinates in the *x*, *y*, or *z* coordinates targeted by both raters [Figure 2, Supplementary Table 2]. The coordinates of these outliers still displayed high intra- and inter-rater reliability (ICCs 0.797-0.998) [Supplementary Table 3].

Table 2. The subjects had an intra-rater distance of 3-4 mm by both raters

Rater	DL-STN	Subject ID	Intra-rater distance		
			x	*y*	*z*
R1	Left	e319	3	0	0
R2	Left	e281	0	4	1
R2	Right	e340	0	-3	0

DL-STN: Dorsolateral subthalamic nucleus; R1: rater 1 (ZN); R2: rater 2 (YJ).

Table 3. The subjects had an inter-rater distance of 3-4 mm at both rating times

Time	DL-STN	Subject ID	Inter-rater distance		
			x	*y*	*z*
1st	Right	e327	-3	-2	-1
2nd	Left	e249	2	-3	-2
2nd	Left	e281	0	4	1
2nd	Left	e325	0	-3	-2
2nd	Left	e420	1	-3	-2
2nd	Right	e249	-1	-3	0
2nd	Right	e340	-1	-4	-1
2nd	Right	e416	-1	-3	-1

DL-STN: Dorsolateral subthalamic nucleus; 1st: the first targeting of DL-STN; 2nd: the second targeting of DL-STN.

The FC of the DL-STN

Overall, the DL-STN has high FC with the motor cortices, including the premotor area (PMA), primary motor cortex (M1), and supplementary motor area (SMA), at both the group level [Figure 3] and the individual level [Figure 4]. All individuals showed significant FC between the DL-STN seed ROI and the lateral motor cortices [Figure 4], with a peak $r > 0.4$ for most subjects [Supplementary Table 4]. For the five subjects who displayed coordinates 2-3 mm from the average DL-STN, the peak r was 0.3-0.9 [Supplementary Table 4]. The results were validated by using the "CC-CAT" plug-in and are displayed in Supplementary Figure 4.

DISCUSSION

We developed an approach, i.e., AutoSTN, to help automatically target individual DL-STNs in the current study. The obtained DL-STN coordinates demonstrated significant FC with motor areas at both the group level and individual level.

The STN and motor pathway

As a crucial nucleus of both the hyper-direct and indirect motor circuits of the cortico-basal ganglia[13,14], the STN mediates inhibitory output from the basal ganglia to motor cortices. Abnormal increased FC between the STN and motor cortices[25,26] existed in PD patients compared with healthy subjects. This abnormally high connectivity may lead to excessive inhibitory outflow from the base ganglia to motor cortices, resulting in hypokinetic movement disorders in PD patients[27].

Automatic targeting of the DL-STN for FC-guided TMS

STN-DBS surgery is a well-established therapy for drug-refractory PD patients. However, it is an invasive approach with a high cost and depends on strict patient screening criteria[5]. Alternatively, rTMS is a noninvasive and low-cost technique and has been recommended for the treatment of PD patients[5-7]. Usually, the conventional stimulation target for rTMS located within the motor cortices[6,7,28] was defined

Table 4. The mean and SD of the DL-STN coordinates

Rater	Time	Left DL-STN						Right DL-STN					
		x		*y*		*z*		*x*		*y*		*z*	
		Mean	SD	Mean	SD	Mean	SD	Mean	SD	Mean	SD	Mean	SD
R1	1st	-12.23	0.88	-14.29	0.84	-6.21	1.07	13.03	0.70	-13.71	0.74	-6.31	1.00
	2nd	-12.01	0.75	-14.24	0.87	-5.95	1.01	12.91	0.76	-13.74	0.81	-6.21	0.93
R2	1st	-11.65	0.83	-14.76	1.08	-6.68	0.99	12.05	0.84	-14.15	0.87	-6.87	0.99
	2nd	-11.65	0.83	-14.76	1.20	-6.77	0.95	12.12	0.77	-14.28	1.01	-6.88	1.03
Overall		-11.89	0.82	-14.51	1.00	-6.40	1.01	12.53	0.77	-13.97	0.86	-6.57	0.99

SD: Standard deviation; DL-STN: dorsolateral subthalamic nucleus; R1: rater 1 (ZN); R2: rater 2 (YJ); 1st: the first time the DL-STN was targeted; 2nd: the second time the DL-STN was targeted.

according to "Hotspot", a brain area corresponding to hand movement. As an individualized variation, the "Hotspot" is not always located within the M1 area[29]. Furthermore, the distance of the "Hotspot" defined according to different sessions would be varied from several millimeters to centimeters[30-32]. Additionally, this defined stimulation method ignores impaired activity because of brain lesions in PD patients. Therefore, individualized stimulation targets are essential for improving the therapeutic efficacy of rTMS for PD patients.

FC-guide rTMS approach could connect a superficial cortex with a core deep brain effective target in DBS surgery, such as the STN or the pallidus pars interna (GPi)[16,33], realizing individualized precise stimulation. Indeed, these effective deep brain targets for DBS were functionally connected with motor cortices. Indeed, these effective deep brain targets for DBS were functionally connected with motor cortices[34]. Furthermore, retrospective studies found that the FC strength between the subgenual anterior cingulate (sgACC) and the dorsolateral prefrontal cortex (DLPFC) was correlated with rTMS clinical efficacy for major depressive disorder (MDD)[35-37]. Moreover, fMRI-guided rTMS has been demonstrated to be effective in the treatment of MDD patients, and this individualized neuronavigational method was represented by Stanford Neuronavigational Therapy (SNT) which has been approved by FDA[38]. In line with numerous previous studies[39-41], we found significant FC between the STN and motor cortices (including M1, SMA, and premotor area). On the basis of these findings, although there was no evidence about FC-guided TMS utilization in PD, we presume that the FC peak within the motor cortices could be used as the superficial stimulation target in rTMS therapy for patients with PD.

However, the STN can be functionally divided into three subregions, i.e., the medial limbic, ventromedial associative, and dorsolateral motor subregions (DL-STN)[42-44]. The DL-STN was the region that provided the maximum therapeutic effect with the least adverse events during DBS surgery[45-47]. Although image-based DL-STN targeting in DBS surgery has been well established with modern MRI techniques, e.g., ESWAN, it is a challenge to manually localize multiple anatomical landmarks.

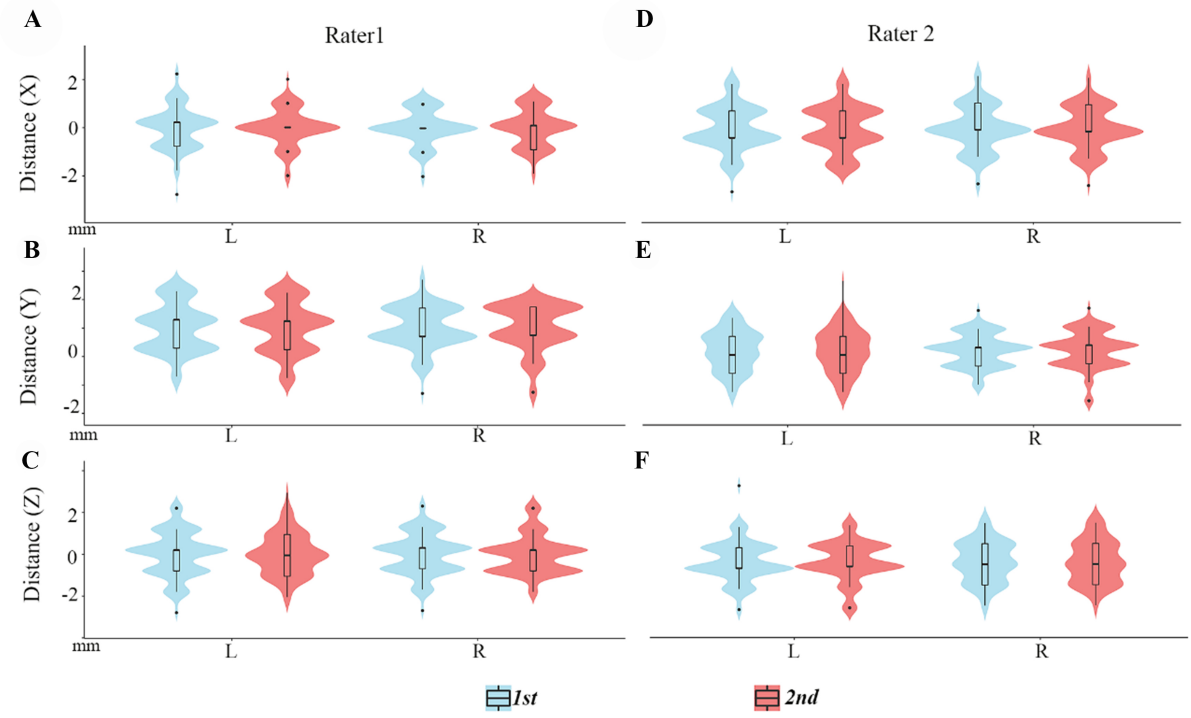

Figure 2. The distances between individual and average DL-STN coordinates in *x*, *y*, and *z*, respectively. (A)-(C) are the results targeted by Rater 1 (ZN); (D)-(F) are the results targeted by Rater 2 (YJ). DL-STN: Dorsolateral subthalamic nucleus.

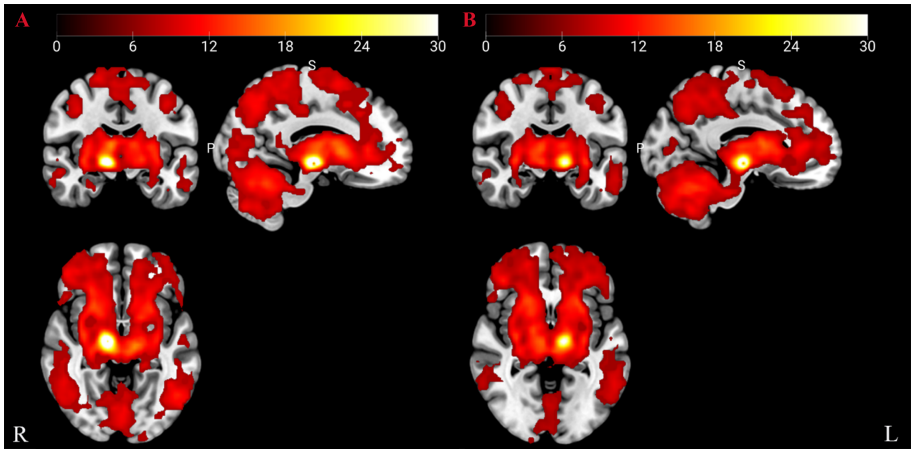

Figure 3. One sample t-tests of the FC of the bilateral DL-STN (GRF correction, individual $P < 1E-09$, cluster $P < 1E-07$). (A) The right DL-STN; (B) the left DL-STN. FC: Functional connectivity; DL-STN: dorsolateral subthalamic nucleus; GRF: Gibbs random field.

Here, we provided an AutoSTN method to automatically localize DL-STN coordinates. The AutoSTN method was performed based on the image-based DL-STN targeting method by manually localizing the DL-STN targets of 78 healthy subjects to obtain the average coordinates. It has been shown that the image-based DL-STN targeting method displayed the smallest variance compared with the indirect targeting method based only on AC and PC landmarks or the image-only direct targeting method, which was closely associated with the optimal electrode contact with satisfactory clinical outcome[21,22]. Our results showed that the DL-STN coordinates had both high intra- and inter-rater reliability (ICC > 0.95). The overall DL-STN

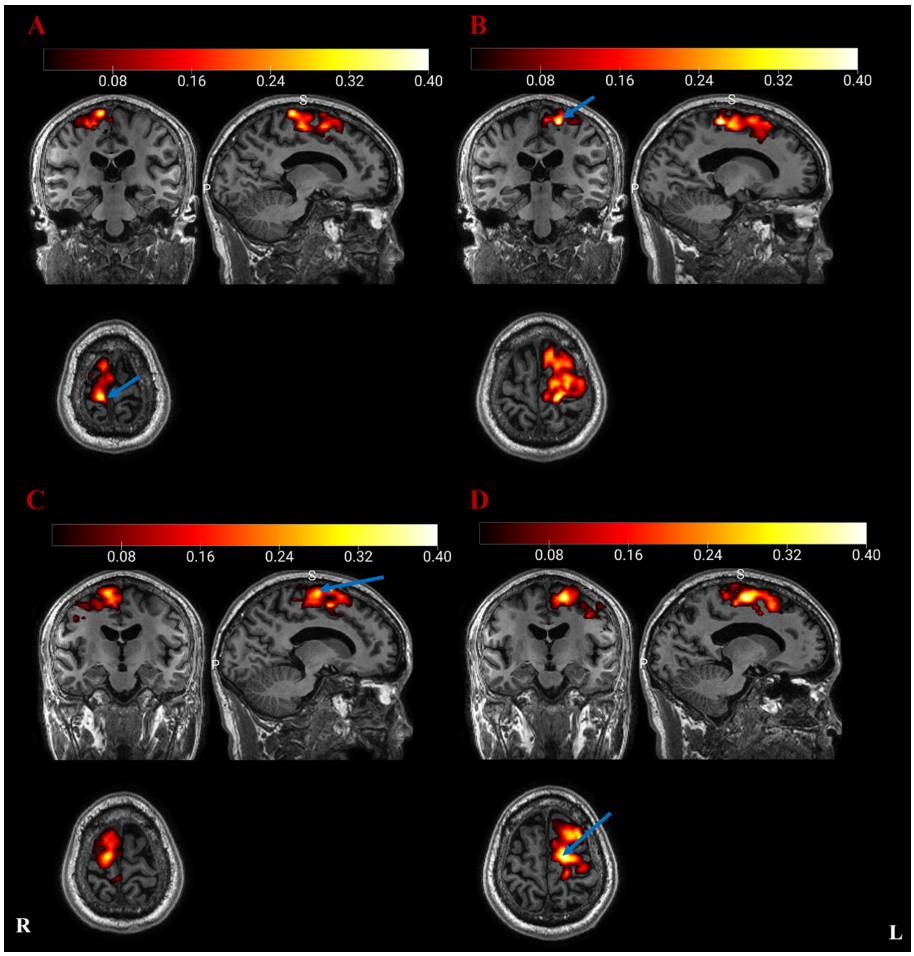

Figure 4. The FC of the DL-STN within the motor cortex in native AC-PC space of one subject; (A) and (B) the FC of the left DL-STN within the left and right hemisphere motor cortices of one subject; (C)and (D) the FC of the right DL-STN within the left and right hemisphere motor cortices of the same subject. The high FC areas indicated by arrows might be potential therapeutic targets for future FC-guided rTMS. FC: Functional connectivity; DL-STN: dorsolateral subthalamic nucleus; AC-PC: anterior commissure-posterior commissure; rTMS: repetitive transcranial magnetic stimulation.

coordinate targeting was in agreement with that of Lozano *et al.*[22] [Supplementary Table 1]. Moreover, most subjects displayed less than 2 mm of the intra- and inter-rater distances of the *x*, *y*, and *z* coordinates [Supplementary Figure 1, Tables 2 and 3].

Only 5 (6.4%) subjects displayed distances in the *x*, *y*, and *z* directions between the individual and the averaged DL-STN coordinates higher than 2 mm but less than 3 mm [Supplementary Table 2]. These five subjects did not display high intra- and inter-rater distances of more than 3 mm. Furthermore, all five subjects showed high FC between the DL-STN and the motor cortices. Collectively, these findings further implied that the average DL-STN coordinates can be used as the coordinates for most people, which allowed for the development of AutoSTN coordinates.

One-stop plug-in for "AutoSTN" implementation

Based on the software RESTplus, we developed a one-stop plug-in toolkit named "CC-CAT" for automatic seed-based FC analysis [Supplementary Figure 2]. As shown in our FC analysis results [Figure 4], future rTMS studies could consider the peak FC coordinates in the motor cortices as stimulation targets for rTMS

therapy. We validated the one-stop plug-in and obtained the same results as those of DPABI [Supplementary Figure 4]. Moreover, the CC-CAT supports any seed-based FC in both individual original space and standard space. Researchers could select the peak FC points in the original space as the individualized rTMS stimulation target.

Limitations and cautions

We strongly suggest that researchers double-check the quality of spatial normalization by visual inspection of the plug-in "CC-CAT", especially for rTMS treatment. The final coordinates should also be double-checked on the structural images. Furthermore, we could not exclude the variations resulting from different MRI machines and settings, and its robustness and adaptability should be explored in the future. Finally, as this study represents only an initial exploration of individualized FC-guide TMS therapy for PD, it did not include any patients with PD. Therefore, the effectiveness of DL-STN FC-guided rTMS as a therapy needs to be investigated in future clinical studies.

Conclusions

In our study, we developed an AutoSTN method to help automatically target the DL-STN, which corresponds to the average coordinates of a group of healthy subjects. Furthermore, based on the AutoSTN coordinates, a one-stop plug-in FC analysis was developed, which could be integrated into future FC-guided rTMS therapeutic procedures.

All original code has been deposited at GitHub and is publicly available at GitHub - Hongy1836/ccat-toolbox.

DECLARATIONS

Authors' contributions

Made substantial contributions to conceptualization, data analysis, and manuscript writing: Zhao N, Qiao Y, Yue J, Jing Y

Made major contributions to manuscript review, editing, and made major contributions to study design: Zhen Y, Xiang YT, Wang J, Zang YF

Performed data acquisition, as well as providing technical and material support: Ge Q, Zhang J, Zhang M

Availability of data and materials

The data that support the findings of this study are available from the corresponding author upon reasonable request.

Financial support and sponsorship

This work was supported by the National Nature Science Foundation of China (NSFC) [81520108016].

Conflicts of interest

All authors declared that there are no conflicts of interest. Zang YF is an Editorial Board member of the journal *Ageing and Neurodegenerative Diseases.*

Ethical approval and consent to participate

The experiment was performed in accordance with the Declaration of Helsinki and approved by the Ethics Committee of the Center for Cognition and Brain Disorders (CCBD) at Hangzhou Normal University (HZNU) (No. 20140508). A written informed consent was obtained from each subject prior to participation in this study.

Consent for publication

Written informed consent for publication was obtained from all participants.

REFERENCES

1. Wirdefeldt K, Adami HO, Cole P, Trichopoulos D, Mandel J. Epidemiology and etiology of Parkinson's disease: a review of the evidence. *Eur J Epidemiol* 2011;26 Suppl 1:S1-58. DOI PubMed
2. Beitz JM. Parkinson's disease: a review. *Front Biosci* 2014;6:65-74. DOI PubMed
3. Rascol O, Payoux P, Ory F, Ferreira JJ, Brefel-Courbon C, Montastruc JL. Limitations of current Parkinson's disease therapy. *Ann Neurol* 2003;53 Suppl 3:S3-12; discussion S12. DOI PubMed
4. Ceravolo R, Rossi C, Del Prete E, Bonuccelli U. A review of adverse events linked to dopamine agonists in the treatment of Parkinson's disease. *Expert Opin Drug Saf* 2016;15:181-98. DOI PubMed
5. Heumann R, Moratalla R, Herrero MT, et al. Dyskinesia in Parkinson's disease: mechanisms and current non-pharmacological interventions. *J Neurochem* 2014;130:472-89. DOI PubMed
6. Goodwill AM, Lum JAG, Hendy AM, et al. Using non-invasive transcranial stimulation to improve motor and cognitive function in Parkinson's disease: a systematic review and meta-analysis. *Sci Rep* 2017;7:14840. DOI PubMed PMC
7. Li S, Jiao R, Zhou X, Chen S. Motor recovery and antidepressant effects of repetitive transcranial magnetic stimulation on Parkinson disease: a PRISMA-compliant meta-analysis. *Medicine* 2020;99:e19642. DOI PubMed PMC
8. Rossi S, Hallett M, Rossini PM, Pascual-Leone A; Safety of TMS Consensus Group. Safety, ethical considerations, and application guidelines for the use of transcranial magnetic stimulation in clinical practice and research. *Clin Neurophysiol* 2009;120:2008-39. DOI PubMed PMC
9. Rossini PM, Burke D, Chen R, et al. Non-invasive electrical and magnetic stimulation of the brain, spinal cord, roots and peripheral nerves: basic principles and procedures for routine clinical and research application. An updated report from an I.F.C.N. Committee. *Clin Neurophysiol* 2015;126:1071-107. DOI PubMed PMC
10. Deng ZD, Lisanby SH, Peterchev AV. Coil design considerations for deep transcranial magnetic stimulation. *Clin Neurophysiol* 2014;125:1202-12. DOI PubMed PMC
11. Obeso JA, Marin C, Rodriguez-Oroz C, et al. The basal ganglia in Parkinson's disease: current concepts and unexplained observations. *Ann Neurol* 2008;64 Suppl 2:S30-46. DOI PubMed
12. Wang JX, Rogers LM, Gross EZ, et al. Targeted enhancement of cortical-hippocampal brain networks and associative memory. *Science* 2014;345:1054-7. DOI PubMed PMC
13. DeLong MR, Wichmann T. Circuits and circuit disorders of the basal ganglia. *Arch Neurol* 2007;64:20-4. DOI PubMed
14. Nambu A, Tokuno H, Takada M. Functional significance of the cortico-subthalamo-pallidal 'hyperdirect' pathway. *Neurosci Res* 2002;43:111-7. DOI PubMed
15. Xie CL, Shao B, Chen J, Zhou Y, Lin SY, Wang WW. Effects of neurostimulation for advanced Parkinson's disease patients on motor symptoms: a multiple-treatments meta-analysas of randomized controlled trials. *Sci Rep* 2016;6:25285. DOI PubMed PMC
16. Peng L, Fu J, Ming Y, Zeng S, He H, Chen L. The long-term efficacy of STN vs GPi deep brain stimulation for Parkinson disease: a meta-analysis. *Medicine* 2018;97:e12153. DOI PubMed PMC
17. Parsons TD, Rogers SA, Braaten AJ, Woods SP, Tröster AI. Cognitive sequelae of subthalamic nucleus deep brain stimulation in Parkinson's disease: a meta-analysis. *Lancet Neurol* 2006;5:578-88. DOI PubMed
18. Schaltenbrand G, Wahren W. Atlas for stereotaxy of the human brain. Georg Thieme. 1977. Available from: https://www.semanticscholar.org/paper/Atlas-for-Stereotaxy-of-the-Human-Brain-Schaltenbrand-Wahren/d181ed3002e0d5c503be5a565e500d1aa181220b. [Last accessed on 8 May 2024].
19. Chandran AS, Bynevelt M, Lind CRP. Magnetic resonance imaging of the subthalamic nucleus for deep brain stimulation. *J Neurosurg* 2016;124:96-105. DOI PubMed
20. Ashkan K, Blomstedt P, Zrinzo L, et al. Variability of the subthalamic nucleus: the case for direct MRI guided targeting. *Br J Neurosurg* 2007;21:197-200. DOI PubMed
21. Andrade-Souza YM, Schwalb JM, Hamani C, et al. Comparison of three methods of targeting the subthalamic nucleus for chronic stimulation in Parkinson's disease. *Neurosurgery* 2008;62 Suppl 2:875-83. DOI PubMed
22. Lozano CS, Ranjan M, Boutet A, et al. Imaging alone versus microelectrode recording-guided targeting of the STN in patients with Parkinson's disease. *J Neurosurg* 2018;130:1847-52. DOI PubMed
23. Koo TK, Li MY. A guideline of selecting and reporting intraclass correlation coefficients for reliability research. *J Chiropr Med* 2016;15:155-63. DOI PubMed PMC
24. Shrout PE, Fleiss JL. Intraclass correlations: uses in assessing rater reliability. *Psychol Bull* 1979;86:420-8. DOI PubMed
25. Fernández-Seara MA, Mengual E, Vidorreta M, et al. Resting state functional connectivity of the subthalamic nucleus in Parkinson's disease assessed using arterial spin-labeled perfusion fMRI. *Hum Brain Mapp* 2015;36:1937-50. DOI PubMed PMC

26. Baudrexel S, Witte T, Seifried C, et al. Resting state fMRI reveals increased subthalamic nucleus-motor cortex connectivity in Parkinson's disease. *Neuroimage* 2011;55:1728-38. DOI PubMed
27. Vitek JL, Giroux M. Physiology of hypokinetic and hyperkinetic movement disorders: model for dyskinesia. *Ann Neurol* 2000;47:S131-40. PubMed
28. Chen KHS, Chen R. Invasive and noninvasive brain stimulation in Parkinson's disease: clinical effects and future perspectives. *Clin Pharmacol Ther* 2019;106:763-75. DOI PubMed
29. Ahdab R, Ayache SS, Brugières P, Farhat WH, Lefaucheur JP. The hand motor hotspot is not always located in the hand knob: a neuronavigated transcranial magnetic stimulation study. *Brain Topogr* 2016;29:590-7. DOI PubMed
30. Cincotta M, Giovannelli F, Borgheresi A, et al. Optically tracked neuronavigation increases the stability of hand-held focal coil positioning: evidence from "transcranial" magnetic stimulation-induced electrical field measurements. *Brain Stimul* 2010;3:119-23. DOI PubMed
31. Julkunen P, Säisänen L, Danner N, et al. Comparison of navigated and non-navigated transcranial magnetic stimulation for motor cortex mapping, motor threshold and motor evoked potentials. *Neuroimage* 2009;44:790-5. DOI PubMed
32. Weiss C, Nettekoven C, Rehme AK, et al. Mapping the hand, foot and face representations in the primary motor cortex - retest reliability of neuronavigated TMS versus functional MRI. *Neuroimage* 2013;66:531-42. DOI PubMed
33. Wong JK, Cauraugh JH, Ho KWD, et al. STN vs. GPi deep brain stimulation for tremor suppression in Parkinson disease: a systematic review and meta-analysis. *Parkinsonism Relat Disord* 2019;58:56-62. DOI PubMed PMC
34. Fox MD, Buckner RL, Liu H, Chakravarty MM, Lozano AM, Pascual-Leone A. Resting-state networks link invasive and noninvasive brain stimulation across diverse psychiatric and neurological diseases. *Proc Natl Acad Sci U S A* 2014;111:E4367-75. DOI PubMed PMC
35. Fox MD, Buckner RL, White MP, Greicius MD, Pascual-Leone A. Efficacy of transcranial magnetic stimulation targets for depression is related to intrinsic functional connectivity with the subgenual cingulate. *Biol Psychiatry* 2012;72:595-603. DOI PubMed PMC
36. Weigand A, Horn A, Caballero R, et al. Prospective validation that subgenual connectivity predicts antidepressant efficacy of transcranial magnetic stimulation sites. *Biol Psychiatry* 2018;84:28-37. DOI PubMed PMC
37. Cash RFH, Cocchi L, Lv J, Fitzgerald PB, Zalesky A. Functional magnetic resonance imaging-guided personalization of transcranial magnetic stimulation treatment for depression. *JAMA Psychiatry* 2021;78:337-9. DOI PubMed PMC
38. Paychiatric News. FDA clears accelerated TMS protocol for depression. Available from: https://psychnews.psychiatryonline.org/doi/full/10.1176/appi.pn.2022.10.10.40. [Last accessed on 8 May 2024].
39. Isaacs BR, Forstmann BU, Temel Y, Keuken MC. The connectivity fingerprint of the human frontal cortex, subthalamic nucleus, and striatum. *Front Neuroanat* 2018;12:60. DOI PubMed PMC
40. Shen B, Gao Y, Zhang W, et al. Resting state fMRI reveals increased subthalamic nucleus and sensorimotor cortex connectivity in patients with Parkinson's disease under medication. *Front Aging Neurosci* 2017;9:74. DOI PubMed PMC
41. Wang Z, Chen H, Ma H, Ma L, Wu T, Feng T. Resting-state functional connectivity of subthalamic nucleus in different Parkinson's disease phenotypes. *J Neurol Sci* 2016;371:137-47. DOI PubMed
42. Arnold Anteraper S, Guell X, Whitfield-Gabrieli S, et al. Resting-state functional connectivity of the subthalamic nucleus to limbic, associative, and motor networks. *Brain Connect* 2018;8:22-32. DOI PubMed
43. Brunenberg EJL, Moeskops P, Backes WH, et al. Structural and resting state functional connectivity of the subthalamic nucleus: identification of motor STN parts and the hyperdirect pathway. *PLoS One* 2012;7:e39061. DOI PubMed PMC
44. Lambert C, Zrinzo L, Nagy Z, et al. Confirmation of functional zones within the human subthalamic nucleus: patterns of connectivity and sub-parcellation using diffusion weighted imaging. *Neuroimage* 2012;60:83-94. DOI PubMed PMC
45. Guehl D, Edwards R, Cuny E, et al. Statistical determination of the optimal subthalamic nucleus stimulation site in patients with Parkinson disease. *J Neurosurg* 2007;106:101-10. DOI PubMed
46. Avecillas-Chasin JM, Alonso-Frech F, Nombela C, Villanueva C, Barcia JA. Stimulation of the tractography-defined subthalamic nucleus regions correlates with clinical outcomes. *Neurosurgery* 2019;85:E294-303. DOI PubMed
47. Brunenberg EJL, Platel B, Hofman PAM, Ter Haar Romeny BM, Visser-Vandewalle V. Magnetic resonance imaging techniques for visualization of the subthalamic nucleus. *J Neurosurg* 2011;115:971-84. DOI PubMed